

FEASIBILITY OF PAIRING A LOW-COST POSITIVE DISPLACEMENT PUMP WITH LOW-ENERGY PRESSURE COMPENSATING DRIP IRRIGATION EMITTERS FOR SMALLHOLDER FARMS IN AFRICA

**Seiji Engelkemier
 Fiona Grant
 Jordan Landis
 Carolyn Sheline
 Hannah Varner
 Rebecca E. Zubajlo**

Department of Mechanical Engineering
 Massachusetts Institute of Technology
 Cambridge, MA 02139
 Email: 2.76-fall18-sunculture@mit.edu

**Julia Sokol
 Amos Winter**

Global Engineering and Research Lab
 Massachusetts Institute of Technology
 Cambridge, MA 02139

ABSTRACT

In low income countries, existing drip irrigation systems are cost prohibitive to many smallholder farmers. Companies are working to develop efficient, low-cost irrigation systems by using technologies such as positive displacement (PD) pumps and pressure compensating (PC) emitters. However, these two technologies have not been paired in an efficient and cost-effective manner. Here we describe a proof-of-concept pump control algorithm that demonstrates the feasibility of exploiting the physical relationship between the input electrical power to a PD pump and the hydraulic behavior of a system of PC emitters in order to determine the optimal pump operating point. The development and validation of this control algorithm was conducted in partnership with the Kenya-based irrigation company SunCulture. This control method is expected to reduce cost, improve system efficiency, and increase accessibility of irrigation systems to smallholder farmers.

β	Mechanical coefficient of flow	$rpm\ s / m^3$
β'	Electrical coefficient of flow	$V\ s / m^3$
I	Current	A
k_e	Motor constant	V / rpm
k_t	Motor torque constant	$N\ m / A$
P	Pressure within the hydraulic system	$Pa, m\ (head)$
P_{act}	Activation pressure	bar
Q	Flow rate within the hydraulic system	$m^3 / s, Lph$
R_{motor}	Internal motor resistance	$Ohms$
R_{sys}	Total system resistance	$Ohms$
ω	Motor speed	rpm
τ	Motor torque	$N\ m$
V	Voltage	$Volts$
V_{emf}	Counter electromotive force	$Volts$

NOMENCLATURE

Parameter	Description	Units
α	Mechanical coefficient of pressure	$N\ m / Pa$
α'	Electrical coefficient of pressure	V / Pa

1. INTRODUCTION

1.1 Market Background & Motivation

A growing population, changes in available water supply, and global climate shifts are collectively increasing the need for effective irrigation technologies that conserve water and improve crop yield throughout the world. Driven by these factors, the

global “smart irrigation”¹ market has seen substantial growth over the last decade and is expected to continue to grow with a compound annual growth rate of 18.14% over the next 4 years, reaching a total market size of \$1.51 billion by 2020 [1]. The scale of farming activities varies substantially across different regions of the world. One important subset of the global market is the developing-world market, which accounts for over 1.5 billion people [2]. This subset, in contrast to industrial farming, is made up of mostly smallholder farmer households [2]. In Africa and Asia, 94% and 59%, respectively, of cultivated lands are not currently irrigated [2]. Major companies such as Jain Irrigation Systems Ltd. are providing solutions for this market. Smaller players in the market, such as the Kenya-based company SunCulture, are providing a more targeted approach to increase smallholder farmer access to efficient irrigation systems.

SunCulture has developed targeted products and services for smallholder farmers in Kenya, Uganda, Tanzania, and Zambia, and is developing pilot programs in eight other countries. Despite offering financing options and a lower price point than most competitors, the cost of their current system is still too high for widespread adoption among potential users. Based on a market assessment for Kenya done by CrossBoundary, SunCulture’s existing system has an addressable market size of \$1.06bn. Lower cost products would expand this addressable market and encourage adoption of the technology among smallholder farmers.

1.2 System Technologies

SunCulture currently pairs a positive displacement (PD) pump with drip tape and a water storage tank that acts as a buffer between the pump and the drip tape. PD pumps are constant flow devices that ideally release a fixed volume of water per rotation of the internal mechanism. PD pumps are advantageous because they are highly efficient and work well for low flow rate applications. Currently, in order to provide the necessary flow rate to the customers’ farms, the pump moves water to a tank between the water source and the field. The tank is elevated on a stand to provide the pressure necessary to supply flow to the entire field at a relatively constant pressure. However, this tank makes up more than 50% of the system capital cost (Figure 1).

An existing alternative to drip tape is pressure-compensating (PC) emitters. PC emitters are flow control devices that maintain a constant flow above a rated activation pressure (P_{act}). This contrasts with drip tape, where flow rate is dependent on pressure losses across the system. PC emitters enable effectively uniform irrigation across a field, regardless of distance from the pump, pressure losses along a line, or elevation changes. Irrigation systems do exist that pair a centrifugal pump with PC emitters [3] or combine a PD pump with drip tape [4]. These are widely used by SunCulture and other companies in the industry. However, to the authors’ knowledge, PD pumps and PC emitters have not been paired before due to the challenge of

syncing two flow control devices. Given the unique hydraulic characteristics of each farm, it is difficult to accurately predict a priori what pumping power will be necessary to achieve P_{act} at the furthest emitter. Operating a PD pump at a power where all emitters are above P_{act} drastically reduces overall system efficiency and can damage the system.

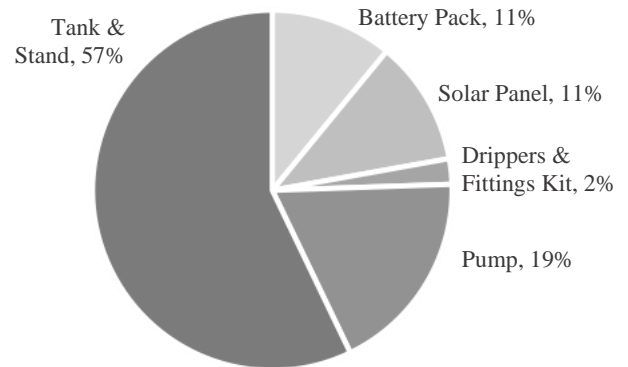


Figure 1 Cost breakdown of components in SunCulture’s drip irrigation system. The tank and stand account for the majority of the system cost.

If the PD pump were directly paired with this PC emitter technology, the tank could be eliminated while maintaining the performance of the current SunCulture drip system. Figure 2 shows the typical setup of a SunCulture irrigation system, including where the tank is currently situated in the system and where the new components would be located.

The feasibility study described here explores the pairing of a low-cost PD pump and low activation pressure PC emitters while preserving the efficiency gains of using a PD pump over a centrifugal pump. The study was conducted in partnership with SunCulture to develop a proof-of-concept showing that a PD pump can be paired with PC emitters to reduce total system cost while meeting key design requirements outlined in Section 1.3.

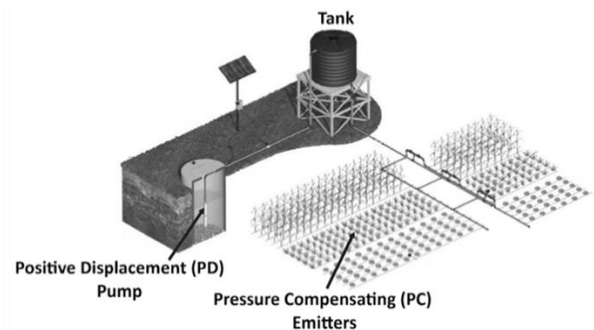


Figure 2. Location of components on a small-acreage farm [2]. By pairing a PD pump with PC emitters, the tank can be eliminated to lower the system cost.

¹ Smart irrigation refers to systems that use external data from weather forecasts, soil conditions, and evaporation and plant water use, to optimize the irrigation system performance.

irrigation flow, based on local weather. These systems are connected via cellular network and update a central system with operating data and weather data. The pumps and panels can be triggered remotely via push notifications from a centralized server. This makes the SunCulture system ideally suited for an additional control method that could regulate the pump operating point to dynamically find and maintain the necessary flow rate of a drip irrigation system using PD pump and PC emitters (PD-PC system).

1.3 Design Requirements

The PD-PC system proposed here needed to meet the operational and design requirements of the current SunCulture system. These requirements included cost, installation time, field size, power requirements, borewell depth, and daily water delivery amounts. In addition to the existing requirements, the control system must be able to detect the ideal operating point where all emitters are within $\pm 7\%$ of their rated flow, which is the industry standard margin on the nominal flow rate of PC emitters [5]. These design requirements are outlined in Table 1 with key assumptions explained in Annex A.

Table 1. Design requirements for the PD-PC system.

Parameter	Requirement
Accessibility Target	System cost < \$875 USD [2]
Training Time	Maintain current training time [6]
Operating Point Detection	Error = $\pm 7\%$ of the rated emitter flow rate [7] [5]
Typical Bore Well Depth	Maximum pump depth = 100 m [2]
System Volume	Maximum volume of system $\sim 0.4 \text{ m}^3$ [6]
Installation Time	Maintain current installation time [6]

2. CONTROL SYSTEM DESIGN THEORY

2.1 System Overview

In order to understand how the coupled PD-PC system would behave, the two technologies were first studied independently. The SunCulture RainMaker 2 PD pump and low-pressure online PC emitters developed by researchers at the MIT Global Engineering and Research (GEAR) Lab were used for this feasibility study.

2.1.1 PD Pump In the ideal case, a progressive cavity PD pump generates a nearly constant flow rate over a range of pressures when operating at a constant speed. The SunCulture PD pump mechanism consists of a helical screw inside a progressive cavity filled with water. When the motor shaft turns the screw, a fixed volume of water inside the cavity is expelled. The mechanical power of the rotating screw is characterized by the speed and torque applied to the motor shaft. The system converts the mechanical power of the motor shaft into hydraulic power, which is characterized by the flow rate and pressure of the displaced water. In reality, there is some slippage at higher pressures due to the deformation of the cavity and incomplete

seals, which means the volume of displaced water is actually dependent on the hydraulic pressure inside the cavity [8].

2.1.2 PC Emitters PC emitters release a nearly constant flow rate for any pressures above the P_{act} of the emitter. This pressure compensating behavior is due to a flexible membrane that, above P_{act} , gradually restricts flow as pressure increases to maintain the rated flow rate (Figure 3). This constant flow behavior ensures that all crops receive a uniform amount of water even when they are placed along a pipe that has a substantial pressure differential. One drawback of conventional PC emitters is their high P_{act} , which adds to the total pressure difference that a pump needs to overcome, necessitating larger, more costly pumps. Recent research has led to the development of PC emitters with a significantly lower P_{act} [9], enabling their use with lower cost pumping systems. These low-pressure emitters have a flow rate of $8 (\pm 7\%) \text{ Lph}$ above a P_{act} of 0.15 bar, in contrast to commercial emitters, which typically have a P_{act} of 0.5-1.0 bar.

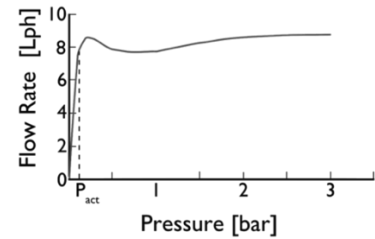


Figure 3. PC emitter behavior for low-pressure PC emitters [9]. After a defined P_{act} , the emitters generate nearly constant flow over a range of inlet pressures.

2.2 Dynamic Power Transfer for PD-PC System

The PD pump is fundamentally an electromechanical device that can be decomposed into the following three subsystems: electrical input, pump motor, and hydraulic network. The physics of each of the subsystems is governed by theoretical equations relating key variables to physical constraints. The electrical power is converted to mechanical power by the motor, which is then converted to hydraulic power by the pump. The electrical power can indirectly be described by Equation (1), where I is electrical current, R_{sys} is the electrical resistance of the system, V is voltage, and V_{emf} is the counter electromotive force that opposes the change in current in the motor, also known as back EMF. The back EMF is proportional to the speed of the motor ω multiplied by the motor constant k_e (Equation (2)). The current (I) is proportional to the torque of the motor (τ) divided by the torque constant (k_t) (Equation (3)).

$$V = IR_{sys} + V_{emf} \quad (1)$$

$$V_{emf} = k_e \omega \quad (2)$$

$$I = \frac{\tau}{k_t} \quad (3)$$

The mechanics of a PD pump ensure a unique relationship between the motor parameters and the hydraulic parameters. By design, the flow rate of a PD pump, Q , is linearly proportional to the speed of the motor, ω . It can also be observed that the motor

torque, τ , is linearly proportional to the pump pressure, P . These relationships are shown in Equations (4) and (5), where α and β are proportionality constants. In effect, the PD pump pressure-flow curves theoretically map onto the motor torque-speed curves. In reality, these relationships are not perfectly linear because the pump flow rate is influenced by pressure due to slippage in the helical mechanism.

$$\tau = \alpha P \quad (4)$$

$$\omega = \beta Q \quad (5)$$

Using Equations (1)- (3), a relationship between voltage, torque, and motor speed can be derived (Equation (6)). A relationship between the input voltage to the motor and the pump pressure and flow rate can then be derived from Equations (4) and (6), shown in Equation (7), where $\alpha' = \alpha R_{sys}/k_t$ and $\beta' = \beta k_e$. Similarly, a relationship between the current draw of the motor and the pressure can be derived (Equation (8)).

$$V = \frac{\tau}{k_t} R_{sys} + k_e \omega \quad (6)$$

$$V = \alpha' P + \beta' Q \quad (7)$$

$$I = \frac{\alpha}{k_t} P \quad (8)$$

Equations (7) and (8) show a key analytical insight: it is possible to relate the electrical inputs to the pump (V, I) directly to its hydraulic outputs (P, Q). This is only made possible by the unique characteristics of a PD pump. It was hypothesized that this theoretical relationship could be exploited to control the PD pump electronically in order to optimize the hydraulic performance of a PC drip system. Assuming the voltage (V) is the primary input to the entire system, if the pump is operating below the activation pressure of the emitters, the flow rate (Q) and pressure (P) are both free to change with small changes in voltage, as shown in Equation (7). However, once the activation pressure is reached, the PC emitters will force the system flow rate to be relatively constant (Figure 3). Any increase in voltage from this point will lead to an increase in pressure, while the flow rate remains constant. From Equation (8), the pressure increase should also be reflected in an increase in the motor current draw (I). Therefore, the current draw of the motor can serve as an indicator to detect the point at which the emitters have reached activation.

This theoretical analysis also makes physical sense. PC emitters are flow control devices. Once the pump surpasses the activation pressure of the emitters, any kinetic energy in the fluid that would have increased the flow rate in a non-pressure compensating system is converted into static pressure at the emitters. This jump in pressure increases the load on the motor, which draws more current in response to the increased hydraulic resistance, provided that the voltage applied to the motor is large enough to allow an increased current draw. However, from a control perspective, it is more convenient to consider the voltage as the input and the PC behavior as the response. This unique system behavior is further explored and exploited to develop a control algorithm that detects the ideal operating point for the PD-PC system.

2.3 Drip System Characterization

To characterize the drip system and its ideal operating point, a typical field in Kenya was modeled. A drip system here is defined as a network of pipes with evenly spaced emitters. The model was used to validate that the tank would not be needed as a flow buffer if the rated outflow from the pump was sufficient to meet the needs of a typical field for a SunCulture customer.

The assumptions used for modeling the field are as follows. A standard plot is approximately 0.2 ha in size with different vegetables (eg. cabbage, tomatoes, and peppers). The emitters currently used by SunCulture are non-pressure compensating and have a flow rate of 0.5 Lph. Pressure compensating emitters were used for our model in order to mimic the target final system. A half to a third of the field is irrigated every day, with the entire plot irrigated over a two to three-day period at a daily water requirement of 5,000-25,000 L/acre/day. The water source for most farms is a well with a depth between 10 to 20 m [10]. Therefore, the chosen drip system was modeled to irrigate a 0.1 ha plot every day to account for the rotating irrigation schedule.

A hydraulics model [11] was used to generate a characteristic system curve. The hydraulics model describes the hydraulic behavior of the system for the given field size, emitter type, total number of emitters, and pipe layout and geometry. The model iteratively calculates the flow and pressure at every point of the system considering the emitter characteristics as well as the pressure losses in the pipes, fittings, and filters. The system curve is characterized by the pressure compensating behavior of the emitters, in which flow is constant once P_{act} is reached.

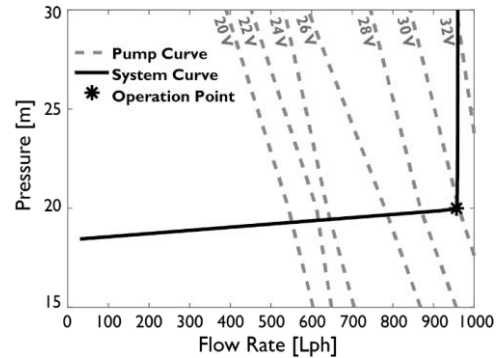


Figure 4. System curve for a typical 0.1-ha plot with a PD pump and PC emitters. The system curve with the ideal (minimum power) operating point is shown overlaid on SunCulture’s constant voltage pump curves.

Figure 4 shows the system curve with pressure and flow gradually increasing until all of the emitters reached P_{act} . At this point, the curve becomes almost vertical, with flow remaining constant over a range of pressures. The ideal operating point of the system curve is also the point at which P_{act} is reached at the emitter farthest from the pump. This is the point at which the minimum power is needed to operate all of the emitters at their rated flow rate. If power is increased past this point, the system will experience an increase in pressure, but the flow rate will remain the same, thereby wasting some energy. If power is

decreased below this point, the flow rate and pressure will decrease and the emitters will no longer uniformly distribute water to the field. The ideal operation point for SunCulture’s standard plot is 960 Lph and 20 m of head (Figure 4).

The system curve was compared to SunCulture’s experimentally-generated pump curves at different input voltages [12]. As shown in Figure 4, the ideal operating point of the system curve intersects with one of the pump curves (at 30 Volts). Therefore, the PD pump could be paired directly with the PC emitters for SunCulture’s typical field size, validating the feasibility of removing the tank from the system.

2.4 Controller Logic

A rudimentary control algorithm is proposed that enables the pump to locate the ideal operating point without a priori knowledge of the hydraulic system. This capability would enable the controller to work for a variety of farms and meet the installation and training design requirements outlined in Table 1. To do this, the controller has to identify the regime change from increasing flow rate to constant flow rate as it moves up the system operating curve (Figure 4). Therefore, the proposed controller design tracks the change in the steady state flow rate of the system to determine where the flow stops changing. This point is where all emitters in the system have reached P_{act} and are emitting water uniformly at the rated flow rate.

In order to meet the requirements of avoiding added cost and complexity, the proposed controller was designed to operate without additional hydraulic sensors. Additionally, the motor controller is inaccessible in the existing SunCulture pump therefore it was assumed the controller could not directly calculate the flow rate from the motor speed. SunCulture does, however, have the ability to control the input voltage and measure the current to the pump from the solar panels.

Given the theoretical relationships between the electrical, mechanical, and hydraulic power (Section 2.2), the current drawn by the motor can be used to detect the point at which the last emitter has reached activation. The behavior of the PC emitters will cause a spike in the system pressure just after all emitters have passed the activation point (Figure 4). This corresponds to a spike in current predicted by Equation (8) as the motor attempts to overcome the sharp increase in the hydraulic load. The control algorithm is designed to detect this spike in current and bring the system back to operate at the voltage just before the spike occurs.

The proposed control algorithm logic flow is shown on the top panel in Figure 5. The algorithm increases the voltage by a user-defined step size (middle graph of Figure 5). A delay (later experimentally determined to be 10 seconds) allows the hydraulic system to reach steady state. The algorithm then measures the current draw of the motor and evaluates the change in current relative to that of the previous step (bottom graph of Figure 5). It was initially proposed that if the change in current is on the same order of magnitude as the previous change, the system has not yet reached activation. The algorithm continues to iteratively increase the voltage until it detects that the change in current is significantly greater than the previous change, as

shown in the “False” pathway in Figure 5. Once the ideal operating point has been surpassed, the current spikes (bottom graph of Figure 5). The controller logic returns a statement of “True,” as the current step is much greater than the previous step, and the voltage is stepped back down to the ideal operating voltage. The controller sets the pump to operate at this point, which ensures the system is operating at activation.

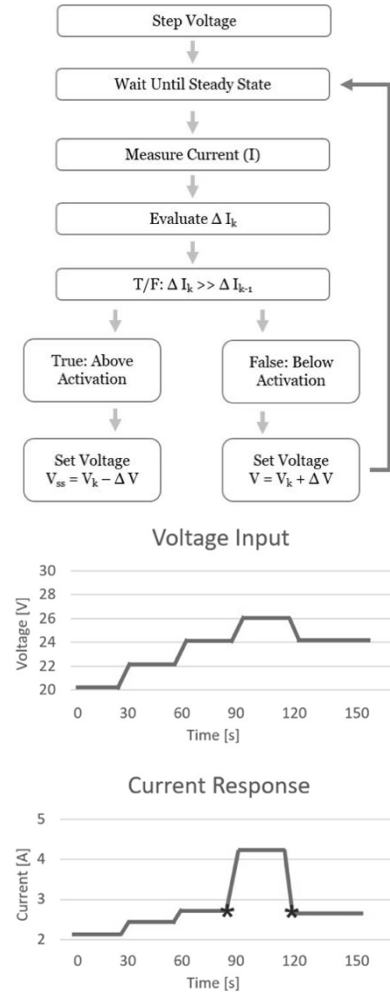


Figure 5. The control algorithm increases the voltage to the pump motor until it detects a sharp increase in current draw. This spike in current corresponds to the spike in hydraulic pressure that indicates the system has just passed the ideal operating point (stars). Once the algorithm detects this spike, it returns to the previous voltage, which enables to pump to operate at the ideal operating point.

This scheme was proposed as a proof of concept for a controller that can independently calibrate a new field or an expanded field. It could also be run periodically throughout the lifetime of the system to detect shifts in the ideal operating point due to emitter clogging or leaks in the pipes and fittings. As the algorithm requires that the input voltage be a free parameter, there must be adequate electrical power available to complete the voltage sweep described above. Further refinement of thresholds and timing is discussed in the following sections.

This scheme was proposed as a proof of concept for a controller that can independently calibrate a new field or an expanded field. It could also be run periodically throughout the lifetime of the system to detect shifts in the ideal operating point due to emitter clogging or leaks in the pipes and fittings. As the algorithm requires that the input voltage be a free parameter, there must be adequate electrical power available to complete the voltage sweep described above. Further refinement of thresholds and timing is discussed in the following sections.

3. METHODS

3.1 Experimental Setup

To characterize the pump and validate the control system, sensors and hardware were installed in a laboratory test system (Figure 6). The electrical hardware consisted of a power supply and pressure and flow sensors. The mechanical hardware consisted of the PC emitters, the PD pump, and connectors (valves, fittings and tubing). These modules integrate with the control algorithm to control the PD pump.

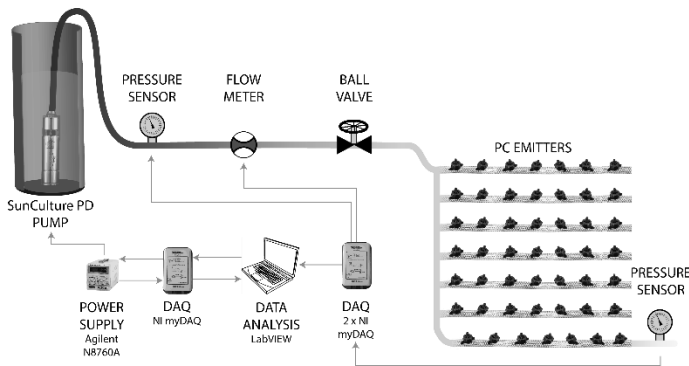


Figure 6. Schematic of the experimental drip system with flow and pressure sensors that allow for simultaneous characterization of hydraulic and electrical parameters of the system. The in-line ball valve and emitter array allow for tests to be performed at various pressures and flow rates.

3.1.1 Electrical Hardware Each component was selected to satisfy the modeled parameters and ranges of variables within the system. Two 0.0 - 10.3 bar pressure sensors (Cynergy 3, Wimborne, UK, ± 0.025 bar error) and a 34 - 4,500 Lph flow sensor (Omega Engineering, Norwalk, CT, $\pm 2\%$ error below 450 Lph, $\pm 1.5\%$ otherwise) were wired into two National Instruments (NI) (Austin, TX) myDAQs. Current and voltage from a 150 V, 34 A power supply (Agilent Santa Clara, CA) was measured by a third NI myDAQ. One of the pressure sensors was installed directly after the pump and the other was placed immediately after the last emitter. The flow meter was installed following the first pressure sensor. NI myDAQ was chosen because it was readily compatible with the LabView Software [2017, National Instruments], which was used to write the control algorithm.

3.1.2 Mechanical Hardware The configuration of the experimental drip system is shown in Figure 7. The SunCulture RainMaker 2 PD pump was placed inside a 1 m³ water tank with hoses connected to transport the water from the tank to a set of

emitters. The pump is rated for 600 Lph and 60 m head and uses a brushless DC (BLDC) motor. A physical system representative of a typical small acreage farm was constructed with a ball valve and emitters. The ball valve was used to perform the initial system characterizations as further described in Section 3.2. The lengths of high-pressure polyurethane tubing (outer diameter 1.91 cm, inner diameter 1.27 cm) were selected to ensure fully developed flow for accurate sensor readings.

The PC emitters used in the experimental setup were online emitters with a rated flow rate of 8 Lph and a 0.15 bar P_{act} . These emitters were designed by researchers at the MIT GEAR Lab and manufactured by Jain Irrigation, Ltd. using their standard injection molding and assembly process [13]. The emitter pipe network included five looped pipe sections (Figure 7). Each section of pipe had a set of 32 PC emitters, except for the first inner section with 24 PC emitters. These loops could be added to or removed from the system to simulate different field sizes depending on the test being performed, as discussed in Section 3.3.

The emitter pipe network was developed to allow for a range of field sizes and flow rates to be tested in a lab setting with limited space. The straight section of pipe with emitters are representative of straight laterals in a field and the 180-degree bends could be representative of frictional and minor losses in a drip system.

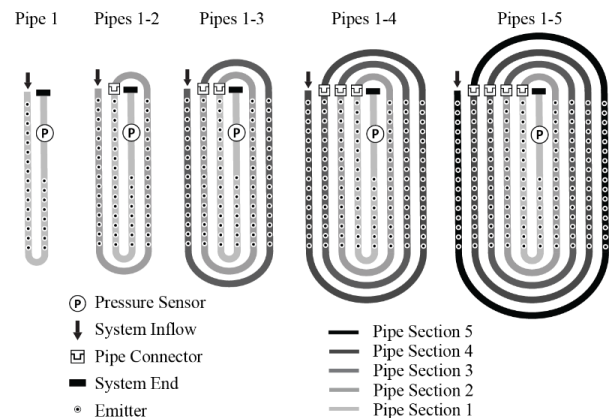


Figure 7. Schematic of variations of the experimental setup showing disconnect points and numbered pipe sections. The set up on the left (Pipe 1) has the smallest number of emitters, with an increasing number of pipe sections and emitters in later set ups.

3.2 Pump Characterization

To inform the feasibility of our control algorithm, the PD pump was characterized. Pressure and flow rates were varied by setting a resistance using the ball valve, selecting a voltage, and then measuring the steady state flow. Pump curves were then generated to characterize baseline performance and capabilities of the PD pump (Figure 8). Figure 8 (a) shows that as voltage increases, the flow rate increases at each pressure. The efficiency of the pump was calculated by dividing the input electrical power by the output hydraulic power; the efficiency curves are shown in Figure 8 (b). The peak efficiency of $\sim 35\%$ is achieved at 32 V with a flow rate around 700 Lph.

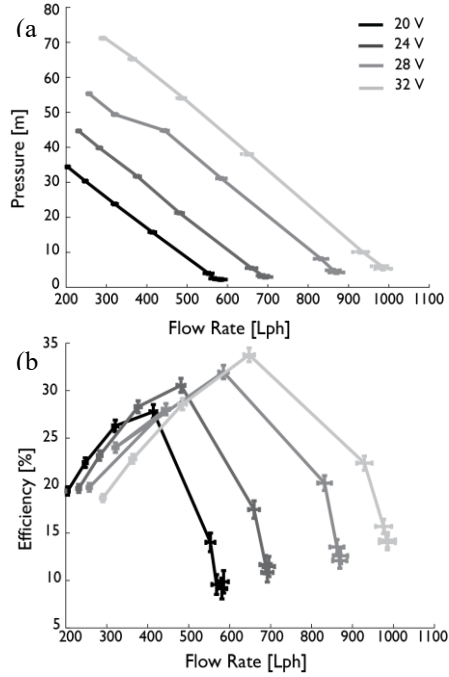


Figure 8. (a) Pump curves were generated experimentally for the SunCulture PD pump to characterize the system and inform the controller design. Voltage was held constant for each curve, while the pressure was adjusted using the inline ball valve, and the steady state flow rate was measured. These curves map to the torque-speed curves of the pump BLDC motor due to the linear relationship between the hydraulics and motor parameters described in Section 3.2. (b) The corresponding efficiency curves of the pump (mechanical power output per electrical power input) show peak efficiencies between 28-35%.

3.3 Drip Characterization

The experimental setup included five pipe sections that could be connected in series to simulate five different field sizes (Section 3.1). The total flow rate, in Lph, was calculated by multiplying the total number of emitters used in each experiment by their rated flow (8 Lph); the total flow for each configuration is shown in Table 2.

Table 2 also shows an estimation of the different field areas that can be approximated from the five experimental setups. For this calculation, typical layout and water requirement parameters were assumed (Section 2.3). The emitter spacing and flow rate were assumed to be 0.5 m and 0.5 Lph, respectively. The lateral spacing and length were assumed to be 1 m and 48 m, respectively. An example field layout is shown in Figure B1 in Annex B. To describe the field area in the experimental set-up please refer to Annex B.

Table 2. Approximate field sizes used in the experimental setup.

Experimental Setup	Pipe 1	Pipes 1-2	Pipes 1-3	Pipes 1-4	Pipes 1-5
Total Flow Rate [Lph]	192	448	704	960	1216
Field Area Equivalent [ha]	0.01	0.04	0.07	0.09	0.12

3.4 Step Response with Emitters

Before designing the control algorithm, the behavior of the system was explored through a series of step response experiments. A fluid network of emitters, spaced evenly along lateral pipes, was connected to the pump to simulate a small field. The connectors between pipes, described in Section 3.1.2 and shown in Figure 7, were adjusted to simulate different field sizes. As the voltage supplied to the pump was varied, the response of the motor current draw, system flow rate, and pressure in the fluid network were measured. The voltage was increased in 1 and 2 V steps between 20 V and 40 V, which is the recommended operating range of the pump [10].

The first set of experiments was performed with different numbers of pipes connected, effectively changing the field size. The second set of experiments was performed with different pre-loads on the hydraulic system by partially closing off the ball valve after the pump. This second set of experiments simulated different well depths. The aim of these experiments was to determine how the hydraulic system responded to step changes in voltage, and therefore power to the pump, in different configurations. The response of the hydraulic system, and in particular the flow rate, was analyzed to determine how quickly the system settled after changing the input voltage to the motor.

3.5 Adaptive Control

After assessing the characteristic response of the system to changes in voltage, a basic control algorithm was developed (Section 2.4) to validate that the ideal operating point of the pump for a given hydraulic system. The control algorithm was developed in National Instruments LabView 2017. The algorithm controlled the voltage of the power supply and measured the current draw of the motor in order to implement feedback control, as diagrammed in Figure 5. To validate the algorithm performance, the system flow rate and pressure, and the pressure after the last emitter were measured outside of the control loop. Before starting the algorithm, the pump was turned on at 20 V, air bubbles were expelled through a release valve at the end of the drip system, and the hydraulic system was allowed to reach steady state. Controller experiments were run with three pipe segments connected and no valve preload, as shown in Figure 7. The aim of these experiments was to determine if the control algorithm could find and maintain the ideal operating point for a given hydraulic system.

4. RESULTS

4.1 Step Response with Emitters

4.1.1 Overall System Behavior The first step in validating the feasibility of an adaptive control system for the PD-PC system was to characterize the behavior of the system and the magnitudes of the anticipated responses. Figure 9 shows the results of one characterization experiment performed on an emitter system with a rated flow rate of 704 Lph. The voltage step size was controlled manually with a target step of 1 V between 20 and 30 V and dwell time of 1 minute at each voltage. The large increase in the terminal pressure sensor reading seen just after 400 seconds indicates that the last emitter in the line

surpassed P_{act} between 26 and 27 V. As the voltage increases beyond 26 V, the flow rate remains stable for the system, as expected due to the pressure compensating behavior of the emitters, whereas the pressure and current continue to rise. This can also be seen by comparing Figure 9 to Figure 4. PC emitter behavior in both cases the flow remains constant ($\pm 7\%$) after activation is reached. Both the motor current and system pressure display a noticeable change at activation.

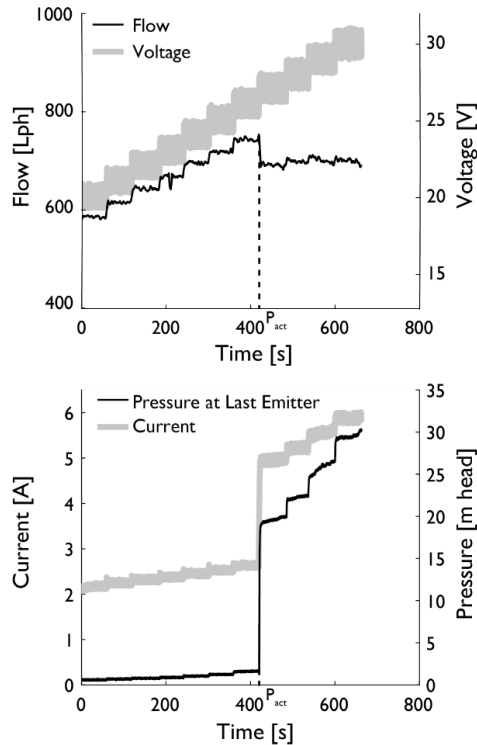


Figure 9. Validation of dynamic power transfer relationships for a PD-PC emitter system with 704 Lph flow rate. The response of the system to all emitters reaching their activation pressure is visible in the significant rise in both pressure and motor current when the input voltage reaches 26 V.

4.1.2 Sensitivity to Flow Rate Alteration Following the demonstration that current and pressure were correlated, a series of sensitivity analyses were performed in order to assess how robust the response was to changes in flow. First, the flow rate of the system was changed from 704 Lph to 960 Lph by connecting a different number of emitters to the test setup, as described in Section 3.1.2. The corresponding responses in current and pressure for the two flow rates are visible in Figure 10, including a sharp increase in current as P_{act} is achieved.

Of note is the non-uniformity of the current step responses for the 960 Lph field size prior to full system activation. The current displays two distinct steps of larger magnitude than the preceding steps (at the dotted lines on Figure 10, top); however, the terminal pressure response does not indicate that P_{act} was achieved until the second of the two current steps (Figure 10, bottom). The first large step occurred at the same voltage as with the 704 Lph field, and the second occurred once activation was completed for the whole system.

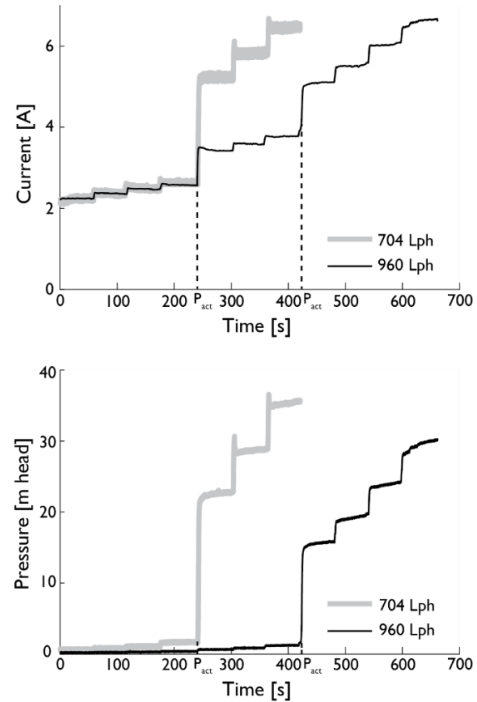


Figure 10. Response of current and system pressure at two field sizes defined by 704 and 960 Lph. The input voltage was increased in 2 V steps to measure the response.

It is hypothesized that this behavior can be explained by the physical layout of the test setup depicted in Figure 7, which included several sharp bends in the pipes. This geometry creates significant pressure losses around the 180-degree bends at each end of the set up. While a step of 1 V on the 704 Lph field was sufficient to elevate the pressure of the entire system above P_{act} simultaneously, 1 V was not sufficient to do the same once the additional pipe section was connected in the 960 Lph flowrate system. Instead, the system displays partial activation where the first portion of emitters were activated, followed by three additional steps whereby the system stagnated as the pump worked to overcome the pressure differential across a bent pipe section, the finally attained P_{act} across all emitters at the final voltage step. A layout that more closely resembles that of a field may not experience this “batch” activation of emitters. Section 4.3 and 5 discuss the implications of this behavior if it is observed in a fielded system.

4.1.3 Sensitivity to Static Head Alteration A second sensitivity analysis was performed to test the system response when the pump was subjected to increased pressure. The aim was to simulate the well being placed at depth in a well. For the same flowrate emitter network, it was observed that the same step in current at activation was seen for pumps that were subjected to increased pressure. Annex C further describes the testing that was performed to validate this result.

4.2 System Characteristics

4.2.1 Motor and Hydraulic Subsystem Relationship In an ideal system, the flow rate is directly proportional to the back

EMF (Section 2.2), the pump slippage is negligible, and the system resistance (R_{sys}) is constant. Using Equations (1), (2), and (5) for these ideal assumptions, the flow rate should scale linearly with the motor current draw for a constant input voltage. (Equations (9) - (10)). The coefficients of Equation (10) were found using a curve fitting tool in MATLAB 2018a where $\beta' = k_e\beta$. The results, shown in Table 3, indicated high fit levels ($r^2 > 0.996$) yielding a range of 103.0 - 108.7 (V s/L) for β' and 1.249 - 1.591 (Ω) for R_{sys} .

$$V - V_{emf} = IR_{sys} \quad (9)$$

$$V - \beta'Q = IR_{sys} \quad (10)$$

Table 3. Motor and Hydraulic Subsystem Coefficients

Variable	Test 1 Fit (95% CI)	Test 2 Fit (95% CI)
β' (V s/L)	108.7 (104.6, 112.7)	103.0 (99.15, 106.9)
R_{sys} (Ω)	1.249 (1.001, 1.497)	1.591 (1.397, 1.786)
r^2	0.9663	0.9770

The aim of this analysis was, first, to determine if the relationship between the hydraulic system and the motor is linear and, second, to determine the current response at the ideal operating point when flow rate becomes constant. In reality, system resistance R_{sys} is not constant as the motor resistance is influenced by motor current draw, and the coefficient of flow (β) scales with the hydraulic pressure due to slippage between the rotor and stator in the pump. The fit indicates that the relationships are linear enough to develop a control algorithm based on these responses.

4.2.2 Power Subsystem Response The results detailed above validate that the electrical behavior of the pump provided sufficient resolution to perceive activation of the hydraulic system, though more data would be required to create a robust predictive model of the behavior. Annex C and D detail the nature of the current responses (including magnitude and rise time) seen for the specific test system used in this work. Rise time was calculated as the time it took for the signal to go from 10% of the signal average from the previous 6 seconds to 90% of the average value for the 6 seconds following the step; 6 seconds was used to obtain the full rise and account for steady state. The activation point was taken as the time at which the terminal pressure sensor in the array of emitters achieved P_{act} .

The system behavior was separated into three regimes—before, at, and after activation of the emitters. For the experiments performed in this study, on average, the change in current per unit change in voltage (dI/dV) is 15.3 times greater at activation compared to that prior to activation for a system with minimal applied static head. This change in current per volt is 6.8 times greater in systems with a static head, as shown in Annex C. The change in current per volt is 2.71 times greater after activation than prior to activation in systems with minimal preload and 1.7 times greater in preloaded systems. This demonstrates a clear trend of the change in current per volt being

smallest in the regime prior to activation, significantly greater as P_{act} is first exceeded, and slightly larger than in the first regime after activation. The authors anticipate that with further study it would be possible to predict the magnitude of this change based on a field size and well depth.

Prior to activation the average rise time was 3.32 s for a system with a minimal preload applied to the pump and 5.00 s for a system with applied preload. At activation, the times were 5.09 s and 4.72 s, respectively, and after activation they were 5.48 s and 6.1 s, respectively. Both of these findings informed the construction of the control algorithm described in Section 4.3.

4.3 Control System

The controller successfully located the ideal operating point of the pump for the 704 Lph hydraulic system with no preload. The controller increased voltage in 2 V steps, and at 26 V, all the emitters in the system reached P_{act} . This can be seen in Figure 11, where the next step up to 28 V produced a sharp increase in pressure and, therefore, the current draw of the motor. In order to bring the system back to the activation pressure, 0.15 bar at the last emitter, the controller had to overcome a hysteretic effect observed in the system. The controller stepped back down to the activation voltage, 26 V, but the last emitter was still above the activation pressure. The current was also higher than it was prior to activation. The controller then reduced the voltage to 20 V, well below activation, then returned to the identified activation voltage, 26 V. At this point, the current and pressure at the last emitter indicated the system was at the ideal operating point, as seen in Figure 11. This hysteretic effect was observed during the experiments, and the controller was modified accordingly to obtain the result described.

The exact source of the system hysteresis is not clear from these experiments, but it is hypothesized that a combination of the tight 180-degree bends in the pipe, the large pipe connectors between the pipe sections, and perhaps the emitters themselves contributed to this behavior. This phenomenon will have to be further explored with longer testing times and different hydraulic network configurations to determine which components contribute. Regardless of the source, this unexpected system behavior indicates that the control scheme may need to be developed further to ensure robust operating point detection for any field and hydraulic network configuration.

As shown in Figure 9, the controller obtains the operating point within the $\pm 7\%$ error band of the emitter flow rate as demonstrated for the 704 Lph field. This result fulfills the “operating point detection” design requirement described in Table 1.

In the case of the 960 Lph field with the “batch” activation behavior, the change in current just after activation is large enough to detect with this algorithm. It would also be trivial to add a stipulation in the control logic that the controller complete its voltage sweep and select the last spike in current as the point of activation. However, given that this behavior could have been an artifact of the experimental setup, further testing should be conducted before modifying the algorithm. The difference in the

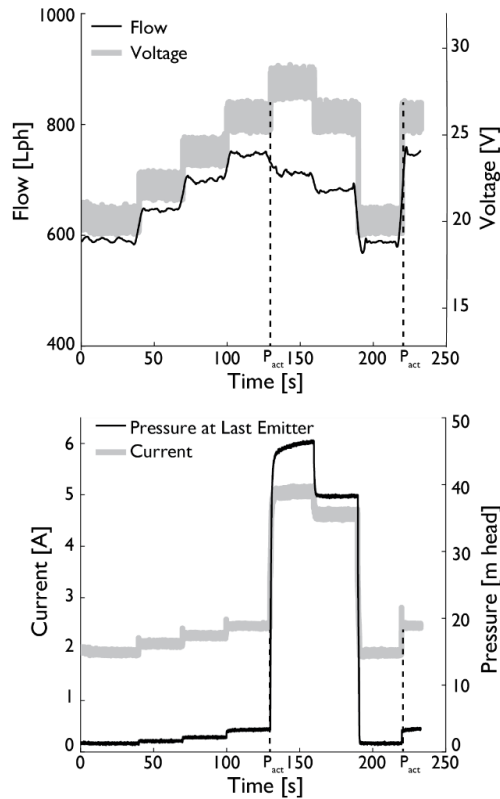


Figure 11. Controller steps up the voltage and monitors current in order to detect the activation point, which occurs just before the sharp increase in current. The controller navigates back to the ideal operating voltage, just before the spike, in a series of steps that overcome the hysteretic system behavior.

response of the two experimental “fields” does highlight an important point: as field size increases, the size of the voltage step may have to increase in order to detect the spike in hydraulic load after activation. This is due to the fact that the emitters are not perfectly pressure compensating and have some error in the theoretically constant flow rate regime. A more sophisticated algorithm that address this hypothesis is proposed in Section 5.2.

By returning the system to a voltage that produces the rated flow without exceeding P_{act} , the controller succeeds in conserving the total power used by the system. Figure 12 shows the power-saving benefits of the controller for flow rates of 704 Lph and 960 Lph by charting the power required to provide an additional unit of flow above and below the activation pressure of the systems.

In both cases, as the voltage is stepped up and the pump begins to operate above P_{act} , the amount of power per unit increase in flow rate increases. For a farmer, this control system not only reduces the system cost by eliminating the tank, it also decreases energy consumption by efficiently using electricity.

5. CONCLUSIONS

5.1 Design Validation

In collaboration with SunCulture, the authors demonstrated the feasibility of using a control algorithm to pair PD pumps with

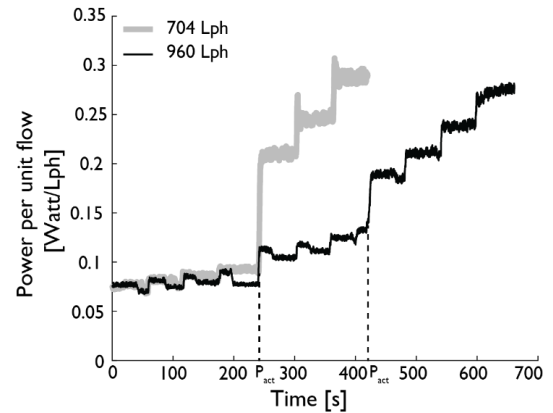


Figure 12. Power consumed per unit flow increases sharply after emitter activation.

PC emitters in a drip irrigation system. The proposed control algorithm can identify the ideal operating point of the pump electrically—solely by controlling the pump voltage and monitoring its current response—without requiring information about the number of emitters, field size, or layout. This allows the PD-PC system to be responsive to a range of field types without adding complexity to the customer experience. The control algorithm could allow SunCulture to eliminate the tank from their irrigation system and lower the total cost, while reducing power consumption, making drip irrigation systems more affordable overall. This concept was validated with tests that established scaling factors between electrical current and flow rate across a range of pressures and flow rates. The control algorithm was successful in an experimental setup with flow rates and pressure losses comparable to typical farms in SunCulture’s customer base.

5.2 Future Work

The authors plan to continue working with SunCulture to refine the control scheme in order to make it more robust and integrate it into the SunCulture’s existing data collection and control architecture. To account for situations where P_{act} is not achieved at a uniform rate due to system layout, the controller may be modified to step through the entire voltage range of the power supply and compare all of the resulting current steps. The controller could then refine the voltage step size and identify when the last group of emitters is activated.

Future improvements to the control scheme may also include development of a continuous monitoring protocol to detect drift from the operating point or any errors initiated by external changes to the irrigation system such as clogged emitters or system malfunction. As SunCulture’s cloud-based data architecture allows for periodic data transfer between each connected irrigation system, integration of the control algorithm will allow for the future application of machine learning techniques. Finally, the team plans to work with SunCulture to perform pilot studies to test the control algorithm in the field.

ACKNOWLEDGMENTS

The authors would like to acknowledge Charles Nichols and the rest of the SunCulture team for their partnership and support on this research. The authors would also like to acknowledge the MIT Global Engineering teaching team and support staff for all of their input and guidance. Finally, the authors would like to acknowledge the National Instruments Applications Engineering Team and Xiang Zhang for their assistance troubleshooting data acquisition and software challenges.

REFERENCES

- [1] Reuters. 21 August 2017. "Smart Irrigation Market Size, Share, Report Analysis, Trends & Forecast 2022". Available at: <https://www.reuters.com/brandfeatures/venture-capital/article?id=14906> (Accessed: 15-Dec-2018).
- [2] SunCulture. April 2018. Company Presentation Deck. Private Communication.
- [3] Dripdepot. 26 October 2018. "Water Pump Buying Guide. Available at: <https://help.dripdepot.com/support/solutions/articles/11100006172-water-pump-buying-guide> (Accessed: 15-Dec-2018).
- [4] SunCulture. n.d. "How it Works, SunCulture technology changing lives". Available at: <http://sunculture.com/how-it-works> (Accessed: 15-Dec-2018).
- [5] International Organization for Standardization. "Agriculture irrigation equipment – Emitters and emitting pipe – Specification and test method" (Standard 9261:2014).
- [6] Ibrahim, Samir. 3 May 2016. "SunCulture Annual Letter 2016". Available at: <https://medium.com/@samiribrahim/sunculture-annual-letter-2016-ccfa78e45f62> (Accessed: 15-Dec-2018).
- [7] Sokol, Julia et al. Energy Reduction and Uniformity of Low-Pressure Online Drip Irrigation Emitters in Field Tests. In preparation.
- [8] Zheng, Lei, Wu, Xiaodong, Han, Guoqing, Li, Huachang, Zhuo, Yi, and Zhou, Dake. "Analytical Model for the Flow in Progressing Cavity Pump with the Metallic Stator and Rotor in Clearance Fit". Hindawi. *Mathematical Problems in Engineering*. Volume 2018. Article ID 3696930. <https://doi.org/10.1155/2018/3696930>
- [9] Shamschery P, Wang R-Q, Tran DV, Winter V AG. (2017) Modeling the future of irrigation: A parametric description of pressure compensating drip irrigation emitter performance. *PLoS ONE* 12(4): e0175241. <https://doi.org/10.1371/journal.pone.0175241>
- [10] Nichols, Charles. 26 September & 2 November 2018. CTO and Co-founder. SunCulture, Nairobi Kenya. Private Communication.
- [11] Grant, Fiona, Sokol, Julia, Sheline, Carolyn, and Winter, Amos G. "Development of a System Model

for Low-cost, Solar Powered Drip Irrigation Systems in the Mena Region". *Proceedings of the ASME IDETC/CIE*. DETC2018-86297: Quebec City, Quebec, Canada, August 26-29, 2018.

- [12] Sunculture. September 2018. Pump Curves. Provided by Email Communication.
- [13] Shamschery, Pulkit, and Winter, Amos G. "Shape and Form Optimization of on-Line Pressure-Compensating Drip Emitters to Achieve Lower Activation Pressure". *ASME Journal of Mechanical Design*. Volume 140 (March 2018).

ANNEX A

DETAILED SYSTEM REQUIREMENTS

Parameter	Requirement	Assumptions
Accessibility Target <i>("Accessibility" to cost sensitive customer base)</i>	System cost < \$875 USD [2]	Eliminating the water tank can reduce the total system cost by ~ 50%.
Training Time	Maintain current training time [6]	N/A
Operating Point Detection	Error = $\pm 7\%$ of the rated emitter flow rate [7] [5]	During experiments, the control algorithm will determine if pump is operating at lowest power point for given system configuration (resistance). Experimentally detect correct operating point to maintain flow rate within $\pm 7\%$ of the rated emitter flow rate [7] [5].
Typical Bore Well Depth	Maximum pump depth = 100 m [2]	Can be used with available water sources; based on current SunCulture specifications [2].
System Volume	Maximum volume of system ~ 0.4 m ³ [6]	"Fit into the back of a Sedan" [6]
Installation Time	Maintain current installation time [6]	N/A

ANNEX B

DRIP SYSTEM CHARACTERIZATION

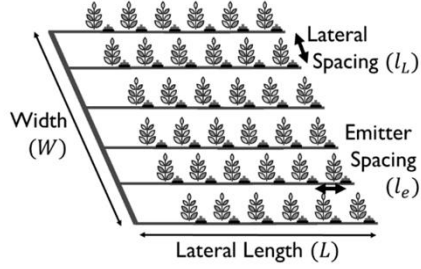


Figure B1. Typical field layout with emitters.

The field area (A) is calculated as shown in Equations (D1) - (D6). Equation (D1) describes the general field area calculation with a unit conversion from m^2 to ha where L is the length of each lateral and W is the field width. Equation (D2) calculates the width (W) based on the number of laterals (N_L) and the lateral spacing (l_L).

$$A = \frac{WL}{10,000} \quad (D1)$$

$$W = (N_L - 1)l_L \quad (D2)$$

Equations (D3) - (D5) calculate N_L by rounding the total number of emitters (N_e) divided by the number of emitters per lateral (N_{eL}) up to the nearest integer. This ensures that all laterals are the entire field length and that A is rectangular. N_e is calculated as the total flow rate divided (Q_{tot}) by the flow rate per emitter (q_e). N_{eL} is equal to the lateral length divided by the emitter spacing on the lateral (l_e).

$$N_L = \text{round} \left[\frac{N_e}{N_{eL}} \right] \quad (D3)$$

$$N_e = \frac{Q_{tot}}{q_e} \quad (D4)$$

$$N_{eL} = \frac{L}{l_e} \quad (D5)$$

Equations (D1) - (D5) are combined to calculate Equation (D6), the field area as a function of the total flow rate and the assumed typical field parameters. Both the total flow and the field area are shown in Table 2 (in the text) for each of the five experimental configurations.

$$A = \left(\text{round} \left[\frac{Q_{tot} l_e}{q_e L} \right] - 1 \right) \frac{l_L L}{10,000} \quad (D6)$$

ANNEX C

SENSITIVITY TO STATIC HEAD ALTERATION

The sensitivity analysis performed to validate the system response when a static head was applied to the pump provided the authors with confidence that the system behavior will persist with deeper water supplies, however the data was not sufficient to derive clear numerical linkages due to the nature of the test set up. Figure C1 compares two test runs at 704 Lph, with and without an applied static head and the signature of a large step in the current response remains visible.

The ability to tune this test was limited by the use of a ball valve to apply the pressure load at the motor given that the pressure induced by the valve is also dependent on flow rate. Before the P_{act} of the system was reached, the flow rate increased as the power to the pump increased, resulting in a corresponding increase in pressure as well over the course of the test. Therefore, using a ball valve is not exactly equivalent to overcoming a height differential, but it allowed for an initial test of how the system would perform under different static head conditions. Despite this limitation, an increased rate of current change per voltage step remains visible both with and without the applied head on the motor (Figure C1).

In the experiments performed on the 704 Lph field the “No Preload” case was measured to be equivalent to 6.6 m static head for the test setup described in Section 3.1, while the “Preload” case was equivalent to 17m and 36.7 m of head at the activation of the emitters for the manual vs automatic controlled systems. The case of “No Preload” described in Annex D was measured to be equivalent to 6.6 m head.

Similar to the 960 Lph system (Figure 10), the system with an applied static head displays a staggered current response prior to the system achieving P_{act} (Figure C1). Again, it is hypothesized that the geometry of the test system resulted in a delay between when P_{act} was achieved in the initial pipe sections and the later pipe sections as the pressure losses due the bends were overcome.

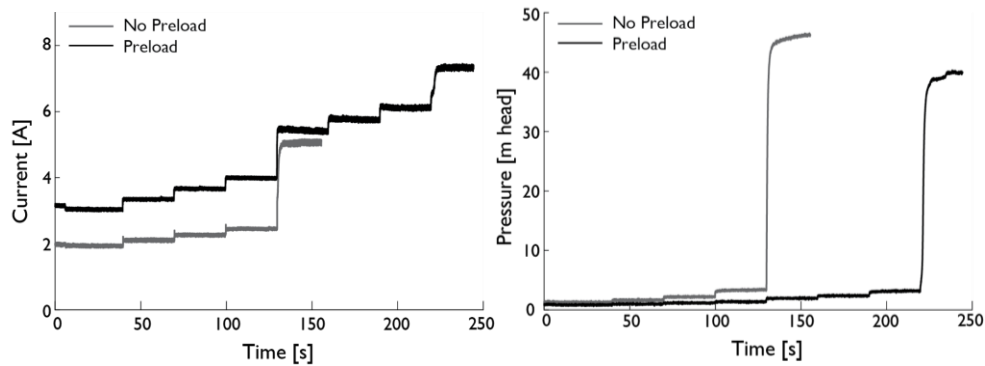


FIGURE C1. Response of current and terminal pressure for two simulated well depths using a ball valve.

ANNEX D

TESTS WITH NO PRELOAD ON MOTOR

Voltage control type	Tested flow rate	Prior to System Activation		At activation		After Activation	
		di/dV ± Stdev (N)	Rise time ± Stdev	di/dV	Rise time	di/dV ± Stdev (N)	Rise time ± Stdev
		[Lph]	[Amps/Volt]	[s]	[Amps/Volt]	[s]	[Amps/Volt]
Manual	448					0.235±0.026 (3)	6.991±0.67
Manual	704	0.074±0.006 (6)	3.85± 1.63	1.900	6.091	0.223±0.013 (3)	4.277±1.01
Auto	704	0.085±0.003 (3)	4.45± 1.09	1.190	4.217		
Manual	960	0.065±0.002 (3)	2.00± 0.39	0.405	4.976	0.184±0.012 (3)	5.179±0.91
Manual	1216	0.130±0.072 (4)	2.96± 0.93				
	Average	0.089	3.315	1.165	5.094	0.214	5.48

TESTS WITH PRELOAD ON MOTOR

Voltage control type	Tested flow rate	Prior to System Activation		At activation		After Activation	
		di/dV ± Stdev (N)	Rise time ± Stdev	di/dV	Rise time	di/dV ± Stdev (N)	Rise time ± Stdev
		[Lph]	[Amps/Volt]	[s]	[Amps/Volt]	[s]	[Amps/Volt]
Manual	448	0.131 (1)	6.35	0.594	6.085	0.235±0.013 (3)	5.871±0.72
Manual*	704	0.140±0.016 (7)	3.85± 1.78	1.094	4.128		
Auto*	704	0.162±0.005 (3)	7.74± 2.65	0.731	2.967	0.263±0.106 (4)	6.325±2.44
Manual*	960	0.151±0.024 (7)	2.06± 0.71	1.210	5.703		
	Average	0.146	5.00	0.907	4.721	0.249	6.10

*As described in 4.1.2, emitters reached activation in batches for the preload tests. For these cases, averages were calculated before the first batch for the “Prior to Activation” data and after P_{act} at the terminal emitter for “After Activation”.